Numerical evaluation of anisotropic fluid flow in sheared rock fractures

doi: 10.1063/1.2721246

Numerical Evaluation of Anisotropic Fluid Flow in Sheared Rock Fractures

K. Nemoto, N. Watanabe, H. Oka, N. Hirano,
and N. Tsuchiya

Graduate School of Environmental Studies, Tohoku University, 6-6-20 Aramaki aza Aoba, Aoba-ku, Sendai, Japan

Abstract. Anisotropic fluid flow in single sheared fractures in granite is investigated numerically under normal stresses up to 90 MPa that are the extended stress conditions of the previous studies. Aperture distributions of the sheared fractures under the normal stresses generated numerically on the basis of direct measurements of contact area suggest anisotropy of connectivity in fracture aperture even under the normal stresses. Numerical simulation of fluid flow using the generated aperture distribution shows not only anisotropy in fracture permeability and that in preferential flow paths, but also the normal stress dependency in the anisotropy of fracture permeability. An investigation on contact ratio reveals the anisotropy and the normal stress dependency in aperture connectivity, which supports the results of flow simulation. These results suggest importance of the flow anisotropy in discrete fractures for investigating three-dimensional flow properties in fractured rocks at a greater depth.

Keywords: Fluid flow, Rock fracture, Anisotropic flow, Aperture distribution
PACS: 91.60.Np

INTRODUCTION

Flow properties in fractures contained in rock are essential for understanding of fluid migration in subsurface rock masses. For instance, accurate prediction of fluid migration in granitic rock masses is required in safety assessments for engineering utilization of underground such as for nuclear waste repositories, oil/gas and geothermal reservoirs. Since permeability of fractures is extremely higher than that of rock matrix in general, fractures behave as major flow paths in the rock masses, which indicates flow properties in fractures is essential for prediction of fluid migration in fractured rocks.

Previous studies on flow properties in single fractures have reported that flow in a fracture forms heterogeneous, anisotropic flow paths, i.e., channeling and tortuous flow [2,15,17-21], which have been attributed to a discrepancy between fluid flow in a parallel plate model and that in a fracture with rough surfaces.

Recent studies on fluid flow in a single fracture have reported anisotropy in permeability of a fracture associated with shear displacement up to several milimeters under normal stress condition up to 10 MPa [1,7,10,12,22]. They concluded that the anisotropy in fracture permeability was caused by anisotropy in contact area distribution of a fracture due to shear displacement.

Under the low normal stress conditions or without normal stress, an increase in volume of aperture due to shearing, i.e., shear dilatancy may be large compared to that of fractures under actual normal stress conditions in underground, since effects of the interactions on fracture surfaces such as deformation or degradation of asperities would be smaller for low normal stress conditions [4,5,7,8] and are expected to be significant under higher stress conditions. Flow properties in single fractures for higher normal stress conditions need to be investigated to evaluate flow properties in fractured rock at a greater depth such as oil/gas and geothermal reservoirs.

CP898, *Water Dynamics: 4th International Workshop on Water Dynamics*
edited by K. Tohji, N. Tsuchiya, and B. Jeyadevan

In this paper, we present results from numerical investigations on anisotropy of fluid flow in sheared fractures under normal stress conditions up to 90 MPa that are the normal stress conditions extended from the previous studies. We simulate a sheared fracture using a tensile fracture on which shear offsets of several millimeters are given before normal stress is applied. First, we show the details of direct contact area measurements in which a pressure-sensitive sheet technique is adopted to detect contact area of the sheared fracture under the higher normal stress conditions. Second, the generation of aperture distribution of sheared fractures is described on the basis of the results from the contact area measurements to investigate flow properties in the fracture through flow simulation. Finally, the results from the numerical simulation of fluid flow in sheared fractures are presented and a correlation between anisotropy in fluid flow and that in the aperture distribution is discussed.

EVALUATION OF CONTACT AREA UNDER NORMAL STRESS USING PRESSURE-SENSITIVE SHEETS

Experimental Technique and Procedure

Figure 1 shows a schematic illustration of the sample assembly and a photograph of the experimental set up. Granite with medium grain (Iidate granite) was used for the experiments for measuring contact area of the sheared fracture. The size of cubic rock samples is 50 mm x 50 mm x 60 mm, containing a single tensile fracture along the horizontal centerline of the sample. Five types of samples containing a single fracture to which shear offsets of 0, 1, 2, 3 and 5 mm were applied were prepared for the experiments.

A pressure-sensitive sheet was inserted between the upper and lower fracture surfaces, which allows direct measurement of contact area in stressed fracture surfaces. Normal stress was applied to the fracture with/without the shear offsets from 10 MPa to 90 MPa sequentially with an increment of 10 MPa for each experimental run using a 25 ton-loading machine. After applying normal stress for 2 minutes, the pressure-sensitive sheet was retrieved from the sample. A steel frame was attached around the fracture to avoid horizontal displacements of the fracture with loading due to the applied shear offsets.

We adopt a commercially available pressure-sensitive sheet (Fuji film Co., FPL-S-MS) because of the simplicity in handling. A pressure-sensitive sheet is comprised of three layers; a dye layer, a developing layer and a base layer [12]. The dye layer and the

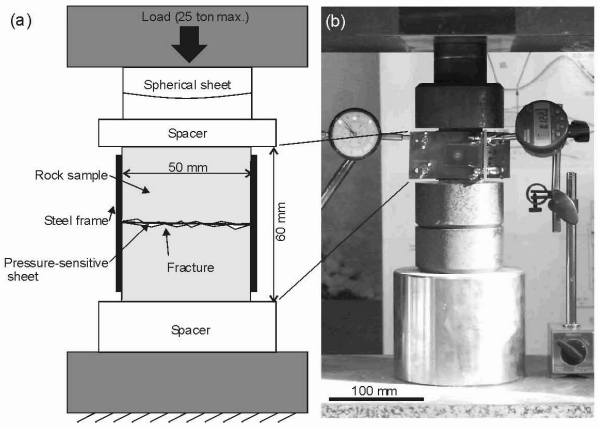

FIGURE 1. (a) A schematic illustration and (b) a photograph of experimental apparatus for the direct contact area measurements.

developing layer are placed on the base layer made of polyethylene terephthalate. The dye layer has microcapsules containing red dye. A pressure-sensitive sheet detects contact areas between objects with the microcapsules rupturing by pressurization to color the developing layer placed under the dye layer. On the catalogue specification, the spatial detection resolution is 0.1 mm x 0.1 mm. Applicable pressure to a sheet is ranged from 10 MPa to 50 MPa and the thickness of a sheet is 0.115 mm.

The thickness of a sheet leads to an overestimate in contact area of a fracture since the sheet detects as a contact area fracture aperture where a gap between the upper and lower surfaces is less than the sheet thickness. Our previous study showed that anisotropy in contact area distribution could be visualized using a pressure-sensitive sheet [12,13], which indicates that uncertainties in detection of the anisotropy in contact area due to the sheet thickness was negligible because entire contact area was much greater than the uncertainties. In the generation of aperture distribution of sheared fractures as described later, we take into consideration the effects of overestimation in contact area due to the sheet.

Procedure for Image Processing

For qualitative evaluation of the detected contact area, an image processing is applied to the sheet images. 8 bit RGB color patterns of the retrieved pressure-sensitive sheet are obtained using a flatbed optical scanner with a resolution of 1200 dpi. The resolution of the image corresponds to a spatial resolution of 0.73 x 0.73 mm. The color images of the pressure-sensitive sheets were converted to 8 bit gray scale images. The intensity distributions (brightness) of the images in gray scale are examined to determine

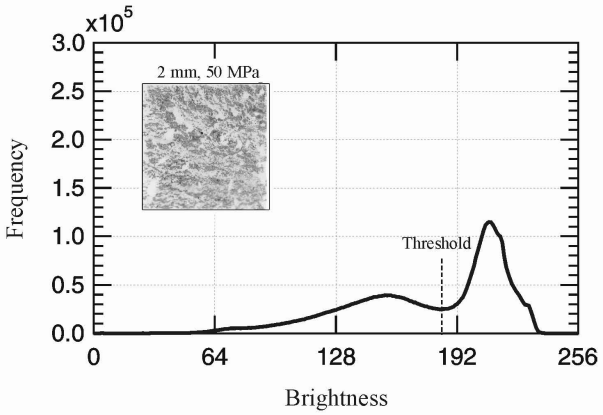

FIGURE 2. A representative intensity distribution of the pressure-sensitive sheet image in gray scale (for shear offset of 2 mm, normal stress of 50 MPa).

a threshold level for converting the gray scale images into binary (black and white) scale.

Figure 2 shows a representative intensity distribution of a sheet image in gray scale. A couple of major peaks can be identified in the intensity distribution. The peak for the lower brightness (the left peak) results from area in contact because the brightness indicates magnitude of pressure acting on the area detected by a pressure-sensitive sheet. The side robe of the left peak (lower brightness) may be due to the uncertainties in the detection due to the sheet thickness. On the contrary, the peak for the higher brightness (the right peak) and its side robe is attributed to a background of the sheet image. The value of intensity at the local minimum between these two peaks could be regarded as the optimum threshold for distinguishing the contact area from non-contact area. A percentage of the contact area is computed by calculating a ratio of the black area in the binary image to an apparent fracture area (50 mm x 50 mm) as a reference for generating aperture distribution for flow simulation.

Generation of Aperture Distribution

Aperture distributions of sheared fractures undergoing normal stress are numerically generated for flow simulation to investigate anisotropy of fluid flow in sheared fractures under the normal stress conditions. Figure 3 shows a procedure for generating fracture aperture distribution on the basis of the results from the direct contact area measurements. The percentages of the contact area are referred for generating aperture distribution of the fractures. Topographies of upper and lower surfaces of a tensile fracture are measured with a 3D laser profilometer [19] with an interval of 0.25 mm over the fracture size of 150 mm x 96 mm. The profilometer has a

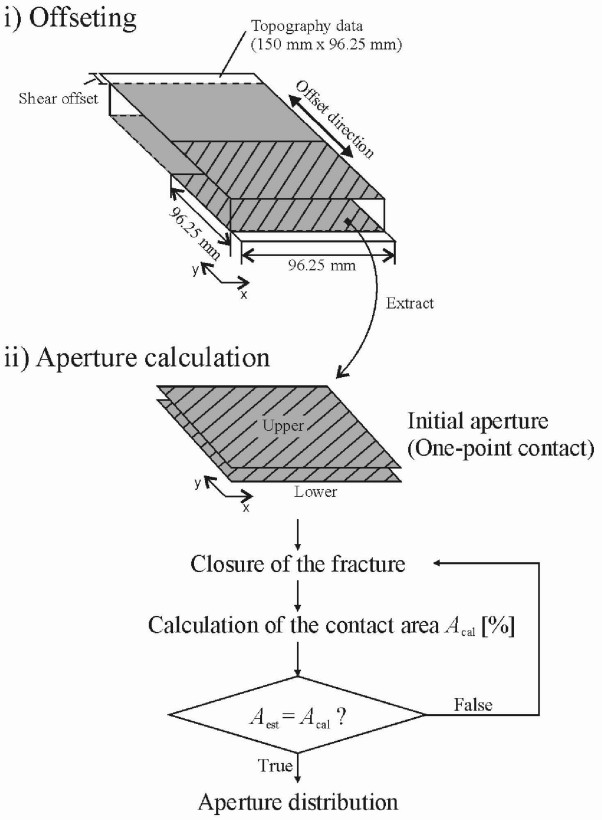

FIGURE 3. Procedure for generating aperture distribution for flow simulation from fracture topography data on the basis of the contact area measurements.

positioning accuracy of ±20 μm in x and y axes and a height resolution of 10 μm in z axis.

An initial aperture distribution of fracture with each shear offset of 1, 2, 3 and 5 mm is generated by applying the shear offsets to one of the topography data. An initial aperture is assumed to be the state of one-point contact indicating the upper and lower fracture surfaces contact each other at a certain point. A distance between the upper and lower surfaces is decreased along the z-axis, and a percentage of the contact area, A_{cal}, is calculated. A_{cal} are compared with the percentage of the contact area computed in the contact area measurements, A_{est}. The closure between fracture surfaces and the calculation of A_{cal} are iterated until A_{cal} become equal to A_{est}. In the calculation of A_{cal}, interpenetrate parts of the fracture surfaces are assumed to be contact areas. It should be noted that A_{est} indicates the percentage of the area where the distance between the upper and lower surfaces is less than the thickness of the pressure-sensitive sheet (0.115 mm). Therefore A_{cal} is computed assuming the aperture area where the distance between the fracture surfaces is less than 0.115 mm to be the contact area.

RESULTS

Contact Area Measurements

Figure 4 shows the binary images of pressure-sensitive sheets for all normal stress and shear offset conditions shown as a function of the applied normal stress in a horizontal axis and the shear offset in a vertical axis. In the binary scale, black areas indicate contact areas, whereas white areas indicate void spaces in fracture aperture. The sheet images for some normal stress and shear offset conditions were not available because the rock samples broke while the load was applied. In Fig. 4, the area of contact appears to increase with increasing normal stress for all shear offset conditions. In contrast, the area of contact decreases with increasing shear offset for all normal stress conditions. In addition to these normal stress and shear offset dependencies in the contact area, patches of contact parts shown as black areas tend to distribute in the direction perpendicular to the shear offset for larger shear offsets.

Figure 5 shows a percentage of the quantified contact area to the apparent fracture area plotted as a function of normal stress for all shear offset conditions. The results show the contact area increases with increasing normal stress for all shear offset conditions. For no shear offset, for example, the contact area increases up to approximately 90% at normal stress of around 50 MPa and keeps constant at 90% for normal stress of over 50 MPa. On the other hand, the contact area decreases with increasing the shear offset for all

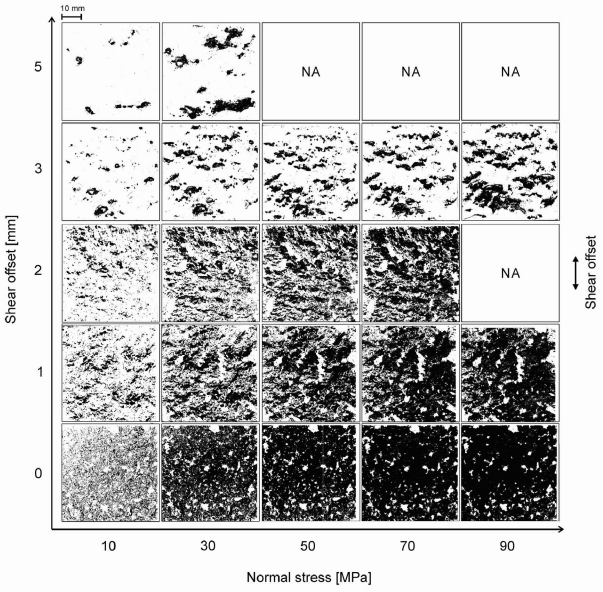

FIGURE 4. Binary sheet images displayed as a function of normal stress and shear offset.

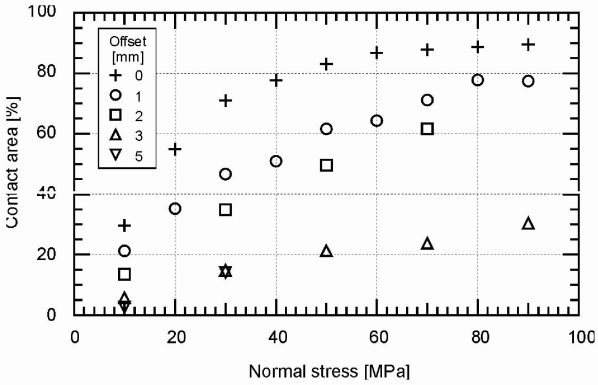

FIGURE 5. Percentages of contact area detected by the pressure-sensitive sheet technique plotted as a function of normal stress for all shear offset conditions.

normal stress conditions. For example, the contact area decreased to less than 20% for the shear offset of 5 mm. Furthermore, the contact area becomes insensitive to an increase in normal stress with increasing the shear offset, particularly in the lower normal stress conditions of less than 40 MPa.

Anisotropy in Aperture Distribution of Sheared Fractures

Figure 6 shows the aperture distribution of the sheared fractures generated on the basis of the contact area measurements. In Fig. 6, the anisotropy in contact area distribution is observed in the generated aperture as well as observed in the direct contact area measurements (Fig. 4) and in other studies [11], which supports the generated aperture distributions are qualitatively valid. In particular, the anisotropic distribution of the contact area is clearly observed for

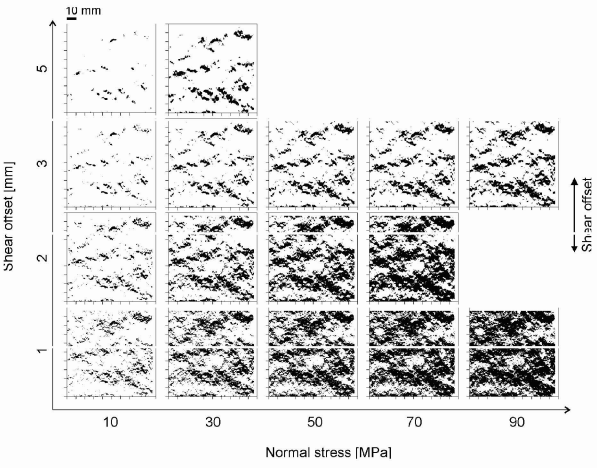

FIGURE 6. Generated aperture distribution shown in binary scale for each normal stress and shear offset condition. Black areas indicate the determined contact areas.

larger shear offsets. In addition, the anisotropic distribution in contact area can be also observed even for higher normal stress up to 90 MPa as clearly observed for the shear offset of 3 mm.

A contact ratio, which is defined as a ratio of contact area for a given direction, is calculated in the both direction perpendicular and parallel to the shear offset to investigate the anisotropy in the aperture distribution. Figure 7a and 7b show the distribution of the contact ratio in the directions perpendicular and parallel to the shear offset for each shear offset condition. The contact ratio in the direction perpendicular to the shear offset (Fig. 7a) shows large variation compared to that in the direction parallel to the shear offset (Fig. 7b) for all shear offset conditions. For example, the variation is larger for normal stress of 70 MPa than that of 10 MPa for the shear offset of 2 mm (Fig. 7a). In addition, the contact ratio in the direction perpendicular to the shear offset (Fig. 7a) shows that a difference between local maximums and local minimums increases with increasing normal stress, and the local minimum values become prominent with the increase in the variation of the contact ratio. The prominence of the lower parts with increasing normal stress can be identified at around 25 mm and 85 mm for the shear offset of 2 mm.

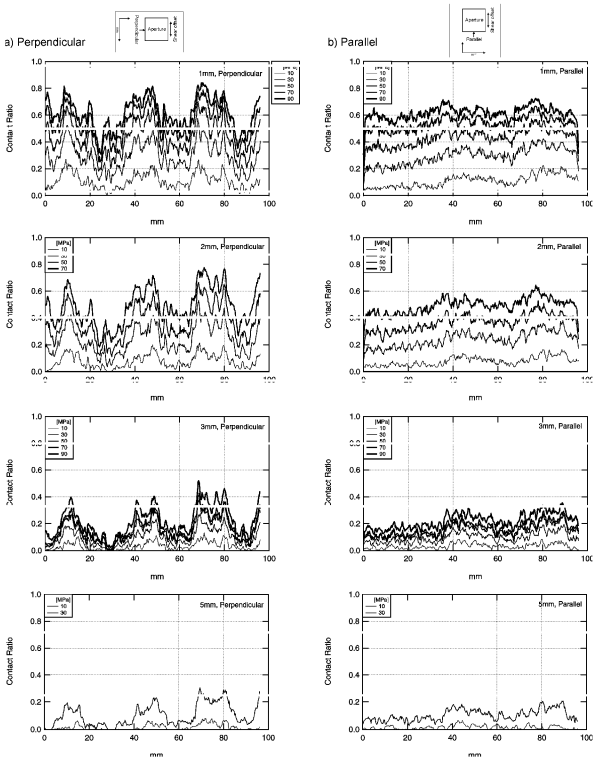

FIGURE 7. Distribution of the contact ratio in the direction perpendicular (a) and parallel (b) to the direction of shear offset for each shear offset condition. The contact ratio is defined as a ratio of contact area on a scan line for a given direction perpendicular or parallel to the shear offset.

NUMERICAL SIMULATION OF FLUID FLOW IN SHEARED FRACTURES UNDER NORMAL STRESS

Flow Simulation

Flow simulations in sheared fractures are carried out using the fracture aperture distribution generated with different shear directions to investigate effects of the anisotropic aperture distribution on fluid flow paths and on possible anisotropy in fracture permeability observed in previous studies [4,11,21]. Flow simulation has been conducted for two different macroscopic flow directions in which parallel and perpendicular to the shear offset direction. Fracture permeability is calculated in the both macroscopic flow directions for all the normal stress and shear offset conditions.

The calculation code of flow simulation is based on the algorithm in the D/SC (Deterministic/Stochastic Crack network modeler) simulation code developed by JAPEX Co., Ltd. The following flow properties such as a flow distribution q_{ij}, fluid pressure distribution P_{ij}, and total flow rate Q at a steady state are calculated by solving the Reynolds equation describing a following two-dimensional equation of continuity at a steady state by a finite difference method [19].

$$\frac{\partial}{\partial x}\left(\frac{e_{ij}^{\ 3}}{12\mu}\frac{\partial P_{ij}}{\partial x}\right)+\frac{\partial}{\partial y}\left(\frac{e_{ij}^{\ 3}}{12\mu}\frac{\partial P_{ij}}{\partial y}\right)=0\,, \quad (1)$$

where e_{ij} is a local distance between fracture surfaces of the generated fracture aperture, P_{ij} is local fluid pressure, μ is a viscosity of the fluid. A laminar flow of incompressible fluid is assumed. A μ is assumed to be a viscosity of water at room temperature 1.0×10^{-3} [Pa·s].

Figure 8 shows boundary conditions in the flow simulation for eq. (1). No flow is allowed from the sidewalls parallel to the macroscopic flow direction. A constant differential fluid pressure is given with a uniform fluid pressure of 1 MPa along one side perpendicular to the macroscopic flow direction and 0 MPa along the opposite side of the fracture aperture. Considering a convergibility of the simulation, the aperture width at the contact area is assumed to be 0.001 mm.

Fracture permeability k is calculated from a total flow rate Q obtained by the Darcy's law described as the following equation,

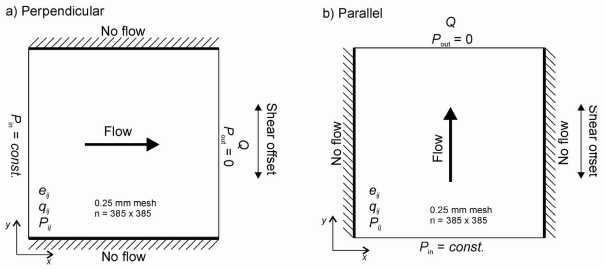

FIGURE 8. Boundary conditions for macroscopic flow directions perpendicular (a) and parallel (b) to the shear offset in the flow simulation.

$$Q = \frac{kA}{\mu}\frac{\Delta P}{L}, \tag{2}$$

where A is a cross sectional flow area, ΔP is a differential pressure and L is a representative fracture length. In a parallel plate model, a relationship between k and hydraulic aperture, e_h, which is defined as a unique distance between fracture surfaces, is given by the following equation,

$$k = \frac{e_h^{\,2}}{12}. \tag{3}$$

The cross sectional flow area A is given by the following equation considering a fracture width W,

$$A = e_h \cdot W. \tag{4}$$

Combining equations (1), (2) and (3), k is given by the following equation [3],

$$k = \left(\frac{\mu L Q}{\sqrt{12} W \Delta P}\right)^{2/3}. \tag{5}$$

Anisotropy of Fluid Flow in Sheared Fractures

Figure 9 shows the calculated flow distribution (q_{ij}) normalized by the maximum value in each flow distribution for the both macroscopic flow directions parallel and perpendicular to the shear offset. In Fig. 9, preferential flow paths, i.e., channeling can be observed irrespective of the macroscopic flow directions for all the normal stress and the shear offset conditions. Meanwhile, the preferential flow paths show lower tortuosity for the macroscopic flow direction perpendicular to the shear offset compared to that for the macroscopic flow direction parallel to the shear offset. This anisotropy of tortuosity in the preferential flow paths is observed for all the shear offset and normal stress conditions. In addition, the flow distribution shows that the preferential flow paths

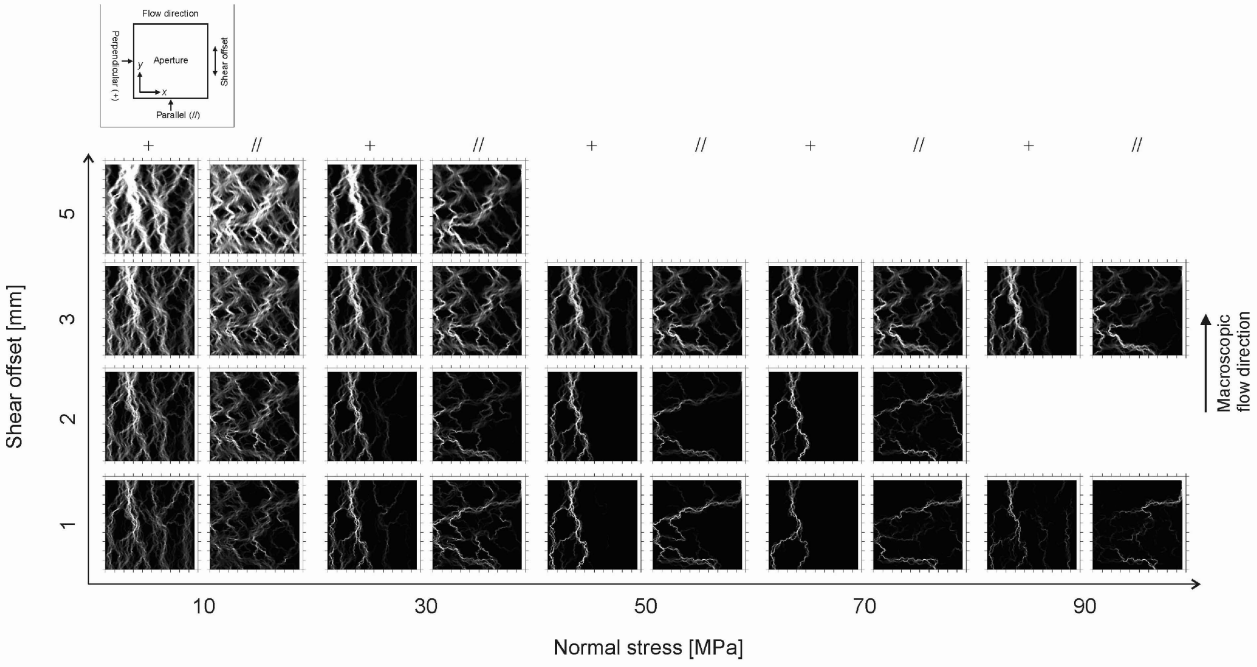

FIGURE 9. Normalized flow distribution obtained by the flow simulation for the macroscopic flow directions perpendicular (+) and parallel (//) to the shear offset.

become narrower and converge in specific flow paths with increasing normal stress for all the shear offsets. In contrast, the width of the preferential flow paths becomes wider and the flow paths are more complicated with increasing shear offset.

The relationship between the fracture permeabilities in the direction parallel ($k_{//}$) and perpendicular (k_{+}) to the shear offset is shown in Fig. 10. The plots distribute below the solid line that shows an equivalent relationship between them in Fig. 10, which indicates anisotropy in fracture permeability and that k_{+} is 1-2 order higher than $k_{//}$ for all cases.

Figure 11 shows a ratio of $k_{//}$ to k_{+} plotted as a function of normal stress. The ratio of fracture permeabilities ($k_{//}/k_{+}$) can be interpreted as a degree of the anisotropy in fracture permeability. The $k_{//}/k_{+}$ shows a tendency to decrease with increasing normal stress for all the shear offsets, which indicates the anisotropy in fracture permeability increases with increasing normal stress.

DISCUSSIONS

Comparison between the flow simulation using the generated aperture distribution and the evaluation of contact ratio indicates that the anisotropy in fracture permeability would be caused by that in contact area distribution due to the shear offset even for normal stress of 90 MPa. The results from contact area measurements showed the anisotropic contact area distribution, i.e., the patches in contact were oriented in the direction perpendicular to the shear offset (Fig. 4). The anisotropy in contact area distribution results in that in aperture distribution, since aperture area in a fracture is regarded as conjugate of contact area.

On the other hand, the evaluation of contact ratio showed the specific parts with lower contact ratio in the direction perpendicular to the shear offset (Fig. 7a), which supports the anisotropy in aperture distribution. Since the contact ratio can be considered to reflect connectivity of aperture, the specific parts with lower contact ratio can be understood as the parts where aperture is highly connected.

The highly connected aperture can be regarded as a transmissive area in fluid flow, which implies preferential flow paths are likely to be formed along it. Hence, it can be considered that the higher fracture permeability was caused by the highly connected aperture formed in the direction perpendicular to the shear offset. In contrast, we can explain that the lower fracture permeability in the direction parallel to the shear offset is because no significant lower parts in the contact ratio were formed in the direction as shown in the contact ratio measurement (Fig. 7b). Thus, we conclude that the anisotropy of fracture permeability observed for the simulated sheared rock fracture under normal stresses up to 90 MPa was caused by the anisotropy of the aperture distribution.

The anisotropy in tortuosity of preferential flow paths (Fig. 4) is also attributed to that in aperture connectivity caused by the anisotropic distribution in contact area. Because of the highly connected aperture formed in the direction perpendicular to the shear offset as shown in the contact ratio, fluid tends to flow in the direction perpendicular to the shear offset. Thus tortuosity in flow paths was lower for the macroscopic flow direction perpendicular to the shear offset, which was the same direction as the highly connected aperture. On the contrary, tortuosity in flow paths was higher for the macroscopic flow direction parallel to the shear offset.

The normal stress dependency in the anisotropy of

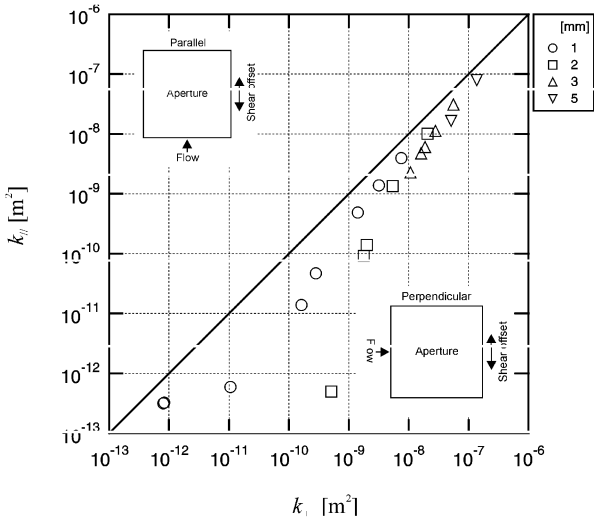

FIGURE 10. Cross plot of the calculated fracture permeabilities in the directions parallel ($k_{//}$) and perpendicular (k_{+}) to the shear offset.

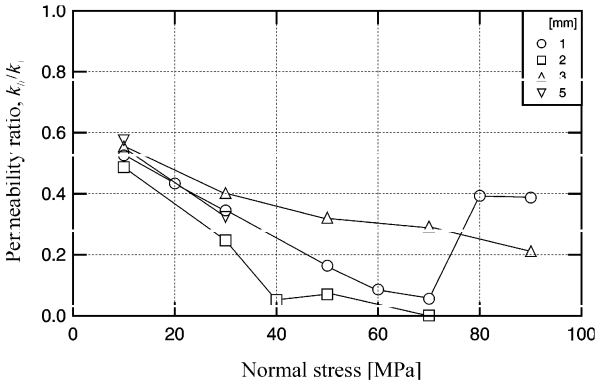

FIGURE 11. The ratio of fracture permeability in the direction parallel to the shear offset ($k_{//}$) to that in the direction perpendicular to the shear offset (k_{+}) plotted as a function of normal stress.

fracture permeability, which was observed as that in the ratio of fracture permeability ($k_{//}/k_{+}$) (Fig. 11), can be explained by the convergence of preferential flow paths on the specific paths with increasing normal stress (Fig. 9). The flow distributions from flow simulation showed the tendency that flow paths converged on certain paths and became narrower with increasing normal stress for the both macroscopic flow directions (Fig. 9). The convergence of flow paths is supported by the prominence of the lower part in the contact ratio with increasing normal stress (Fig. 7a) since preferential flow paths tend to be formed at the lower contact ratio part, thus, are more likely to be formed at the prominent part with increasing normal stress. Permeability of the fracture was strongly controlled by flow properties of the converged paths since they play major role in fluid flow in a fracture. The anisotropy of the converged flow paths such as tortuosity and path width significantly affect that in fracture permeability. Hence, the convergence in preferential flow paths with increasing normal stress is expected to cause the enhancement in the anisotropy of fracture permeability.

It is pointed out that consideration of hydro-mechanical coupled effects on discrete fractures is important for evaluation of flow properties in fractured rock [15]. To extend the investigation on flow properties in fractured rock masses from two dimension [10] to three dimension based on a two dimension estimation, it is important to consider the anisotropy in permeability of discrete fractures, in addition to considering connectivity between fractures that depends on orientation, shape and size of the fractures [10]. Our results show that the anisotropy in fracture permeability due to shear offset exists at relatively high normal stress up to 90 MPa and that the anisotropy in fracture permeability is enhanced with increasing normal stress. These observations indicate that the anisotropy in fracture permeability is not negligible at normal stress conditions at least up to 90 MPa. These results suggest that the anisotropy in fracture permeability should be considered for evaluation of the realistic three-dimensional flow properties in fractured rock masses in addition to closure/dilation of fracture due to normal stress/shear displacement.

CONCLUSIONS

We investigated numerically the anisotropy in flow properties of a single fracture with shear offset through flow simulation using the aperture distribution generated on the basis of the direct contact area measurements of sheared fractures under normal stresses up to 90 MPa.

The results from the direct contact area measurements showed the anisotropic contact area distribution, i.e., the contact areas distributed with the orientation perpendicular to the shear offset, in addition to the decrease with increasing shear offset and the increase with increasing normal stress.

The aperture distributions of sheared fractures were numerically generated on the basis of the contact area measurements. The evaluation of the contact ratio on the aperture distribution revealed that the highly connected apertures were formed preferentially in the direction perpendicular to the shear offset, which supports the anisotropy in fracture permeability and that in tortuosity of the preferential flow paths observed in the flow simulation.

The flow simulation showed that the anisotropy in fracture permeability tends to be enhanced with increasing normal stress for all the shear offset conditions. The normal stress dependency in the anisotropy of fracture permeability was interpreted as a result of the convergence in the preferential flow paths with increasing normal stress. The convergence in the preferential flow paths can be explained by the prominence of the lower parts in the contact ratio in the direction perpendicular to the shear offset with increasing normal stress. The normal stress dependency in the anisotropy of fracture permeability indicates that the anisotropy of fracture permeability could be significant even for higher normal stress at least up to 90 MPa, which implies that it is important to consider the anisotropy of flow properties in discrete fractures for investigating three-dimensional flow properties in fractured rock masses.

ACKNOWLEDGEMENTS

This work was partly supported by Grant-in-Aid Scientific Research from Japan Society for the Promotion of Science (No. 15360472). We thank Dr. Kazuhiko Tezuka (JAPEX Co., Ltd.) and Dr. Kimio Watanabe (RichStone, Ltd.) for providing a simulation code from the D/SC.

REFERENCES

1. Auradou H., G. Drazer, J. P. Hulin, and J. Koplik (2005), Permeability anisotropy induced by the shear displacement of rough fracture walls, Water Resour. Res., 41, W09423, doi:10.1029/2005WR003938.
2. Brown, S., A. Caprihan, and R. Hardy (1998), Experimental observation of fluid flow channels in a single fracture, J. Geophys. Res., 103(B3), 5125-5132.
3. Chen, Z., S. P. Narayan, Z. Yang, and S. S. Rahman (2000), An experimental investigation of hydraulic behaviour of fractures and joints in granitic rock, Int. J. Rock Mech. Min. Sci., 37(7), 1061-1071.

4. Esaki, T., S. Du, Y. Mitani, K. Ikusada, and L. Jing (1999), Development of a shear-flow test apparatus and determination of coupled properties for a single rock joint, Int. J. Rock Mech. Min. Sci., 36, 641-650.
5. Gentier, S., J. Riss, G. Archambault, R. Flamand, and D. Hopkins (2000), Influence of fracture geometry on shear behavior, Int. J. Rock Mech. Min. Sci., 37(1-2), 161-174.
6. Koyama, T., N. Fardin, L. Jing, and O. Stephansson (2006), Numerical simulation of shear-induced anisotropy and scale-dependent aperture and transmissivity evolution of rock fracture replicas, Int. J. Rock Mech. Min. Sci., 43(1), 89-106.
7. Lee, H. S., Y. J. Park, T. F. Cho, and K. H. You (2001), Influence of asperity degradation on the mechanical behavior of rough rock joints under cyclic shear loading, Int. J. Rock Mech. Min. Sci., 38(7), 967-980.
8. Lee, H. S., and T. F. Cho (2002), Hydraulic characteristics of rough fractures in linear flow under normal and shear load, Rock Mech. Rock Eng., 35(4), 299 - 318.
9. Matsuki, K., Y. Chida, K. Sakaguchi, and P. W. J. Glover (2006), Size effect on aperture and permeability of a fracture as estimated in large synthetic fractures, Int. J. Rock Mech. Min. Sci., 43(5), 726-755.
10. Min, K.-B., J. Rutqvist, C.-F. Tsang, and L. Jing (2004), Stress-dependent permeability of fractured rock masses: a numerical study, Int. J. Rock Mech. Min. Sci., 41(7), 1191-1210.
11. Mitani, Y., T. Esaki, and Y. Nakashima (2002), An experimental study on the anisotropy of flow in a rock joint, in Proc. of the 2002 ISRM regional symposium on rock engineering, Seoul, Korea, 281-288.
12. Nemoto, K., H. Oka, N. Watanabe, N. Hirano, and N. Tsuchiya (2005), Measurement of hydraulically ineffective area on a fracture under normal stress condition, Geotherm. Res. Council Trans., 29, 413-417.
13. Nemoto, K., H. Oka, N. Watanabe, N. Hirano, and N. Tsuchiya (2006), Evaluation of fluid flow path in a single fracture undergoing normal stress and shear offset, in WATER DYANMICS: 3rd International Workshop on Water Dynamics, AIP Conf. Proc., vol. 833, edited by K. Tohji et al., 156-161, AIP, New York.
14. Pyrak-Nolte, L. J., and J. P. Morris (2000), Single fractures under normal stress: The relation between fracture specific stiffness and fluid flow, Int. J. Rock Mech. Min. Sci., 37, 245-262.
15. Rutqvist, J., and O. Stephansson (2003), The role of hydromechanical coupling in fractured rock engineering, Hydrogeo. Jour., 11, 7-40.
16. Tsang, Y. W. (1984), Effect of tortuosity on fluid flow through a single fracture, Water Resour. Res., 20(9), 1209-1215.
17. Tsang, C. F., Y. W. Tsang, and F. V. Hale (1991), Tracer transport in fractures: analysis of field data based on a variable aperture channel model, Water Resour. Res., 27(12), 3095-3106.
18. Tsang, C. F., and I. Neretnieks (1998), Flow channeling in heterogeneous fractured rocks, Rev. Geophys. 36(2), 275-298.
19. Watanabe, N., N. Hirano, T. Tamagawa, K. Tezuka, and N. Tsuchiya (2005), Numerical Estimation of aperture structure and flow wetted field in rock fracture, Geotherm. Res. Council Trans., 29, 431-436.
20. Watanabe, N., N. Hirano, and N. Tsuchiya (2006), Determination of aperture structure and fluid flow in a rock fracture under confining pressure through a hihg-resolution numerical modeling on the basis of experimental data, Water Resour. Res., submitted.
21. Yeo, I. W., M. H. De Freitas, and R. W. Zimmerman (1998), Effect of shear displacement on the aperture and permeability of a rock fracture, Int. J. Rock Mech. Min Sci. & Geomech. Abstr., 35(8), 1051-1070.